TIME PROJECTION CHAMBER FOR LOCATING FISSION FRAGMENTS IN RASA FILTERS

William K. Warburton and Brendan J. Dwyer-McNally

XIA, LLC

Sponsored by the National Nuclear Security Administration
Office of Nonproliferation Research and Development
Office of Defense Nuclear Nonproliferation

Contract No. DE-FG02-04ER84179

ABSTRACT

Detecting nuclear debris vented to the Earth's atmosphere from a nuclear explosion can provide highly reliable corroborative evidence that an explosion detected by other means (e.g., seismically) was in fact nuclear. The DOE's Pacific Northwest National Laboratory (PNNL) has developed a highly sensitive, automated system (RASA: Radionuclide Aerosol Sampling and Analysis) to capture such debris from the atmosphere and prescreen it for evidence of radioactivity. RASA is capable of detecting that it has captured as few as 10 fragments, each having only 10^5 fission atoms, in one of its 60 cm x 40 cm polypropylene filters. Having done so, however, RASA lacks the capability of locating these particles, whose sizes will typically be in the 0.3–0.5 μm range, so that they can be excised and distributed to certified laboratories for confirmatory measurements.

In this project we are working to develop an ultra-low background "time projection chamber" to determine the locations of alpha-particle-emitting fragments with a positional accuracy of better than 1 cm. Our work builds upon a commercial product being developed at XIA that is capable of measuring the alpha emissivity of Pb at the 0.0005 α/cm^2/hour level for the electronics industry. Operating as an ionization counter filled with pure N_2, this instrument employs pulse shape analysis to determine if detected alpha particles emanated from the 45 x 45 cm^2 Pb sample or the counter's electrode. This discrimination allows the counter to achieve detection limits that would otherwise require counter construction using hyper-pure materials.

In the time projection chamber we replace the single electrode with an electrode of "flattened" cross-strips that are 1 cm wide. When an alpha particle produces an ionization track in the N_2, the electrons in the track drift to the electrode, inducing currents in the strips as they move. After integration by charge sensitive preamplifiers, the resultant time dependent charge signals are captured by digital signal processors for analysis. Each strip captures the track charge projected on it, and the time of arrival of that charge increases with the distance between its original location along the track and the electrode. By using the complete set of charges and arrival times captured from all the electrode strips, it then becomes possible to reconstruct the original charge track in 3 dimensions. In this paper we present results, computed using an accurate charge induction model, that show the time evolution of the counter's signals and indicate that the method should be able to locate track origins (and hence particle locations) within 0.5 cm using 1 cm strip widths.

OBJECTIVE

XIA, LLC, is currently working to develop an ultra-low background time projection chamber (TPC) to spatially locate the ionization tracks produced by alpha particles emitted from samples placed within it. Accomplishing this project will require meeting multiple objectives including designing and fabricating an experimental TPC, developing electronics to cost-effectively instrument its crossed strip electrode; and, most critical, developing analysis software to extract the track locations from captured signals. In support of the latter effort, we have the objective reported here: to develop a computational procedure capable of producing realistic model electrode signals that we can use both to develop our intuition about the expected signals and, particularly, to provide well characterized input signals for the track location software. Specifically, to test our track location algorithms, we would like to be able to generate expected signals from an alpha particle track emitted from a random location in a random direction within the TPC. Once we can reliably recover track locations from noisy theoretical electrode signals, then we will be ready to move on to examining track signals from point alpha sources—comparing these signals to the theory in order to refine the theory and adapting our location algorithms to accommodate the differences between theoretical and practical signals. In this paper we report that we have successfully developed the theoretical model and present some example signal traces that both elucidate the physical nature of the problem and suggest algorithms that can be developed to extract track locations.

RESEARCH ACCOMPLISHED

Project Background

Detecting nuclear debris vented to the Earth's atmosphere from a nuclear explosion can provide highly reliable corroborative evidence that an explosion detected by other means (e.g., seismically) was in fact nuclear. Under the Comprehensive Nuclear-Test-Ban Treaty (CTBT), the Provisional Technical Secretariat has been building up the International Monitoring System (IMS), including a network of 80 air filtering stations to monitor for radioactive particulate matter. A good example of the instrumentation found at such stations is the highly sensitive, automated RASA (Radionuclide Aerosol Sampling and Analysis) system, developed by DOE's Pacific Northwest National Laboratory (PNNL), which is designed to capture such debris from the atmosphere and prescreen it for evidence of radioactivity (Bowyer et al., 1997; Miley et al., 1998). RASA operates by filtering approximately 20,000 m^3 of air per day through a 60 cm x 40 cm polypropylene filter composed of six 10 cm x 40 cm strips. These strips are piled into a single 10 cm x 40 cm sandwich and wrapped around a 40% HPGe detector to determine if any fission products are present. If any are detected, then the filter is supposed to be divided into 2–3 pieces of nearly equal activity, with 1–2 pieces being sent to certified laboratories for confirmatory measurements and 1 piece being archived. Only this last step (dividing the pieces) is not automated. Personnel have to actually travel to the station to make the division.

RASA is extremely sensitive, being able to detect about 10^6 fission atoms collected in 24 hours, which corresponds to 30 mBq/m^3 of air, for a 20,000 m^3 sample. Its sensitivity is limited by both the efficiency of the HPGe detector and the ubiquitous background of airborne radon daughters (^{214}Pb, ^{214}Bi, ^{212}Pb, ^{212}Bi, and ^{208}Tl) that are also trapped in the filter. The system has no spatial sensitivity. This becomes an issue in the event that a filter needs to be divided, because RASA is sensitive enough to detect as few as 10 particles each containing only 10^5 fission atoms and ranging in size between 0.1 to 10 μm (typically 0.3–5.0 μm). Knowing the locations of these particles then becomes critical: first to know that the number is indeed small, which may require special handling; second, to ensure that each certified laboratory gets an appropriate (and known) fraction of the particulates; and third, because signal to noise in the counting measurements can be increased by over 2 orders of magnitude if the particles can be excised from the radon daughter–laden filter. DOE has therefore included a request in their recent SBIR solicitations for an instrument capable of locating such particles with an accuracy of approximately 1 cm. XIA, LLC, responded to one of these solicitations and is currently doing Phase I research to develop a TPC to meet this need.

Instrument Design

Our TPC design is an extension of an ultra-low background alpha particle counter originally developed to measure alpha particle emissivity from Pb and other materials of interest to the semiconductor industry (Warburton et al., 2004; Warburton and Dwyer-McNally, 2006). The counter is fundamentally a parallel plate ionization chamber with a guard ring enclosing its anode electrode, as shown in the sketch in Figure 1. Both the anode and guard ring are

instrumented with charge integrating preamplifiers whose outputs are digitized and captured for offline analysis. The counter is filled with dry N_2 gas, and 1000 V are applied between the sample tray and the electrodes. When an alpha particle is emitted into the chamber, it deposits energy in the N_2, creating an ionization track. The electrons in the track then drift toward the anode. The operation of the counter is based on the principles of charge induction. As described in the references, in the parallel plate geometry, as long as each electron is drifting toward the anode, it induces a constant current in the anode that, when integrated onto the preamplifier's feedback capacitor, results in a uniformly rising preamplifier output signal. When the electron reaches the anode, the induction stops, no more current flows, and the preamplifier signal either becomes constant or starts decaying (in radiochemical feedback configurations). Thus, the farther the electron drifts, the longer the preamplifier signal risetime and the larger its final value.

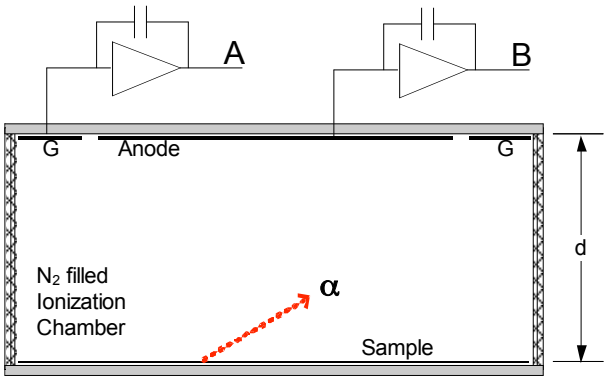

Figure 1. Sketch of the original XIA ultra-low background alpha particle counter.

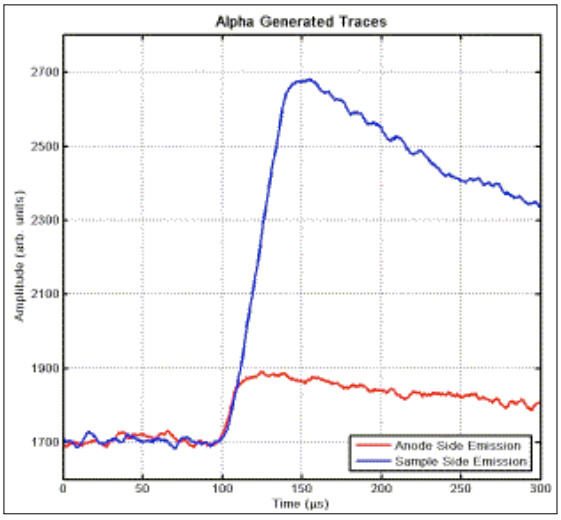

Figure 2. Signal traces captured from the alpha particle counter shown in Figure 1.

In particular, this means that ion tracks emanating on the sample side, which have to drift all the way across the chamber, produce long (45–50 μs) signal risetimes and large output signals. On the other hand, ion tracks that emanate from the anode itself merely have to drift the short distance back to the anode, producing short (10–15 μs) risetimes and small output signals. Figure 2 shows typical traces for both cases. Thus, by measuring signal risetimes and amplitudes, it becomes possible to use pulse shape analysis to discriminate between the two cases and electronically reject signals that do not originate from the sample. By this means it becomes possible to obtain ultra-low background counting without having to construct the counter out of expensive materials having ultra-low alpha particle emissivities. Because alpha particles emanating from the sidewalls can produce signals whose risetimes can have any values lying between the extremes noted above, they cannot be completely rejected based on pulse shape alone. This problem is solved by the use of a guard ring, which is placed to collect a significant fraction of the track charges from all sidewall events. Good anode signals are then required to be in anti-coincidence with guard ring signals. Using these methods we have reduced background counting rates in a commercial prototype having a 45 cm x 45 cm anode area, the Ultra-Lo-1800, to below 0.0001 α/cm^2/hour. This instrument, like the RASA, has no position sensitivity.

In order to add that position sensitivity, we needed to replace the Ultra-Lo's single anode with some type of segmented anode array. After considering the alternatives, we developed the "flattened" cross strip array electrode design shown in Figure 3. The following issues were involved in this decision. First, in order to achieve 1 cm spatial resolution or better, we estimated that we would need pixel dimensions of order 1 cm x 1 cm, or 2400 pixels for the 40 cm x 60 cm RASA filters. However, even at a reduced electronics cost of $500/pixel, this is clearly an enormously expensive approach. At low event rates, where there is never more than a single track in the TPC, a crossed strip design can produce nearly as much tracking information but would require only 100 channels of electronics (40 + 60). While crossed strip anodes are traditionally made of strung wires, our experience with the

Ultra-Lo 1800 showed an extreme sensitivity to microphonics, to which strung wires are particularly prone. The Figure 3 design is fabricated using printed circuit board technology and can be solidly attached to a rigid backing surface, essentially eliminating all but very low frequency pickup. As shown in Figure 3, in one direction there are row electrodes that are actually perforated strips, with preamplifier contacts at one end. The perforations are filled with electrically isolated secondary electrodes that are connected in columns via traces on the board's backside to form the orthogonal set of strips. As the electrons in an ionization track drift toward this anode, they will induce different amounts of charge in different column and row "strips," from which we will attempt to reconstruct the original track location. Our next step, therefore, and the topic of this report, is to develop a model explicitly describing the charge induction process relating the original track location to the strip output signals.

Charge Induction Model

We begin by considering an isolated electron of charge $-q$ located at a distance z from an infinite conducting plane. We know that electric field lines must be everywhere normal to the conductor and that the magnitude of the field as a function of location is easily found using the method of image charges, i.e., by reflecting an image charge $+q$ at a distance $-z$ on the opposing side of the conducting plane. Gauss's Law then provides the connection between the local electric field strength at any point on the conducting plane and the surface charge density σ required to support it. In particular, if we subdivide the conducting plane into a set of strips, pixels, or other shapes, then we can integrate σ_i over any particular isolated shape i to compute the total charge Q_i induced on it.

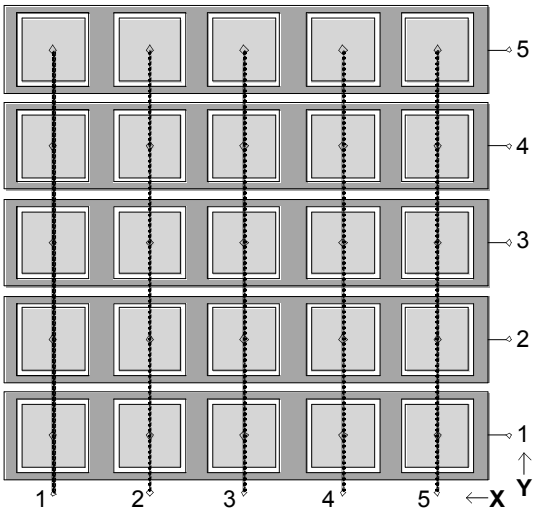

Figure 3. Sketch of the "flattened" cross strip anode.

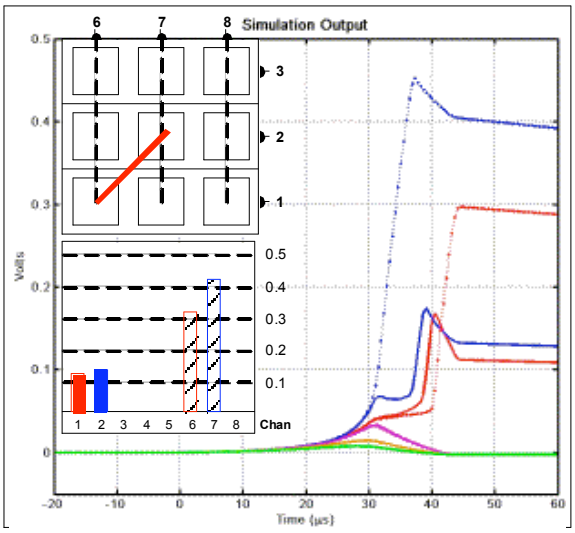

Figure 4. Computed output traces and collected charges for the indicated alpha particle track.

If the separation z is now a function of time $z(t)$, the same procedure can be employed to compute $\sigma(t)$ and hence $Q_i(t)$. The time derivative of $Q_i(t)$ is the current $I_i(t)$ that must flow to the pixel i to allow $Q_i(t)$ to change with time. If this current is integrated by a charge integrating preamplifier, then its output in time will be $Q_{pi}(t) = Q_i(t) - Q_i(0)$. In the case of an ionization track, equal densities of electronic and ionic charge will be created at z at time $t = 0$, but only the electrons will move significantly over the time scales of interest. Thus, the above expression for $Q_{pi}(t)$ will still be valid since only *changes* in surface charge density σ_i cause currents to flow through the external circuit.

When the test charge is placed *between* two planes separated by a distance d, as in our counter, where it lies between the anode plane and the conducting plane of the sample tray, the problem becomes more complex. This is because, while the test charge generates two primary image charges by reflection in the two planes, each of these generates a secondary image charge by refection in the other plane, the secondary charges generate tertiary image charges by reflection and so forth to produce an infinite set of image charges. Luckily, however, when the dimension d is large compared with the pixel or strip dimension, the series converges rather quickly, and typically only the first two or three orders are required to compute σ_i values to better than 1% accuracy. In this case (Warburton, 1998), when the

initial charge is located at *(x, y ,z)* and the ij^{th} rectangular pixel is bounded by the values $(x_{in}, x_{ip}, y_{in}, y_{ip})$, the contribution to the induced charge on the pixel from the k^{th} image charge pair is given by Equation 1, where the fences represent the 4 signed terms from the four limits of integration:

$$Q_{ijk} = \frac{qz}{2\pi}\int_{x_{in}}^{x_{ip}} dx \int_{y_{in}}^{y_{ip}} \frac{dy}{\left(x^2 + y^2 + z_k^2\right)^{.5}} = \frac{q}{2\pi}\left|\left| \sin^{-1}\left(\frac{x_{i\pm}^2 \left(y_{j\pm}^2 - z_k^2\right) - z_k^2\left(y_{j\pm}^2 + z_k^2\right)}{x_{i\pm}^2 \left(y_{j\pm}^2 + z_k^2\right) + z_k^2\left(y_{j\pm}^2 + z_k^2\right)} \right) \right|_{x_n}^{x_p} \right|_{y_n}^{y_p} . \quad (1)$$

Q_{ijk} must then be summed over an adequate number of image charge pairs k to obtain the induced charge on pixel ij. In the present work we used three values of k. Because our strips are not simple rectangles, we computed the induced charge on unperforated strips and on the perforation areas separately. We then subtracted the perforation charges along the row strips to obtain induced charges on the row electrodes and summed perforation charges appropriately to obtain the induced charges on the column electrodes, in both cases from a simple test charge $-q$ at location *(x,y)*.

Having created, in Equation 1, the basic machinery required to compute induced charges on our electrodes, we are now ready to generate signal traces from the drifting charges associated with ionization tracks. We assume that the track emanates from the sample plane at (x_0, y_0), has length L, and forms the angles ϕ with the z axis and θ with the x axis. For want of more-precise knowledge at this time, we assume a uniform charge density along the length L, which will typically be of order 5 cm for typical alpha energies in the 4–6 MeV range. Knowing the energy ε required to form an electron-ion pair in N_2, then gives the charge density ρ along the track. For purposes of computation, the track was subdivided into N equal segments, each of which was then treated as a point charge using Equation 1. A typical value of N in our model was 50. Since the track emanates from the sample surface, there is always at least one track segment that has to drift across the entire distance d = 150 mm, setting a constant maximum drift time T_d = 45 μs at a drift velocity of 0.3 μs/mm. For the purpose of computation, we then divided T_d into M steps, where M was typically 100.

The computation of the electrode signals then was carried out as indicated in the following pseudo code.

For each time step *m* between *1* and *M*, where time step 1 corresponds to the initial condition,
  Transfer $Q_{ij}(m)$ to $Q_{ij}(m\text{-}1)$ for all strip electrodes *ij*
  Zero $Q_{ij}(m)$ for all strip electrodes *ij*
 For each strip electrode *ij*
  For each track segment *n* between *1* and *N*
   Compute *z* of track segment
   If track segment *n* has not reached the anode
    For each image charge pair *k*
     Compute Q_{ijk} using Equation 1 and add to $Q_{ij}(m)$
    End For
   Else If track segment *n* annihilated with its image charge on this electrode
    Add the same charge contribution to $Q_{ij}(m)$ as in previous step *m-1*
   End If
  End For
 End For
  Compute $Q_{pij}(m) = Q_{ij}(m) - Q_{ij}(1)$
End For

Results—Introduction

Figure 4 shows the results of a sample computation using our model code. The inset in the upper left of the figure shows a sketch of a small section of the anode, with three horizontal Row electrodes labeled “1” through “3” and three vertical Column electrodes labeled “6” through “8”. Superimposed on this sketch is the upward projection, along the z axis, of the alpha particle ionization track being computed. Track locations are specified by their x and y point of emanation, measured in millimeters, from the origin (lower left-hand corner of the electrode), their angle θ

from the x axis, and their angle ϕ from the vertical. All tracks are 4.5 cm long. This particular track is designated (5.00, 5.00, 45, 20), meaning that it originated at a point located 5 mm in both x and y (i.e., centered on the first perforation in Column 6) and made angles 45° with the x axis and 20° with the z axis. The superimposed image clearly shows the x, y, and θ values; ϕ can be inferred from the relative track length.

The traces on the right-hand side of the image are the computed preamplifier output signals. The track starts drifting at time $t = 0$, but as is clear from the traces, no significant signals can be seen until approximately 25 μs have passed (i.e., the closest part of the track to the anode has moved over half way across the chamber). This is a manifestation of the well known "small pixel effect" (Barrett et al., 1995), which arises from the fact that until the charge is relatively close to the anode, most of its field lines terminate on other points on the (semi-infinite) anode plane. As may be seen from the figure, the uppermost charges in the track, which lie under Column 7, arrive first, followed by the charges lying under Row 2, Row 1, and Column 6. The sharp rising edges on these traces make it easy to determine which parts of the track arrive first and, thereby, which end of the track is up. The declines on Traces 1, 2, and 7 before they reach their final values at 44 μs is due to the loss of charge induced on their associated electrodes by the charge under Column 6, as that charge is eventually collected onto Column 6. Similarly, the moving track charges temporarily induce charges on Row 3 and Column 8 but leave no net charge on them because no part of the track finally reaches them. The bar graph inset in the lower left of the figure shows the final charges collected by the different electrodes at time 45 μs, just after the last charges in the track complete drifting to the anode.

Results—Variations with Track Orientation and Location

The following figures show how the output traces and collected charges vary as we systematically adjust the location and orientation of the ionization track. In Figures 5A–5C, we move the origin of the track by plus and minus increments of 2.13 mm with respect to a track similar to the one shown in Figure 4, leaving its orientation unchanged. As is immediately obvious, even these relatively small motions produce large changes in the output traces. Thus, compared with the central trace from a (5.00, 5.00, 32, 20) track, the trace from the (2.87, 5.00, 32, 20) track has nearly halved the charge collected on Row 1 and doubled the charge collected on Column 6, while leaving the order of arrival unchanged. On the other hand, the trace from the (7.13, 5.00, 32, 20) track has nearly doubled the charge collected on Row 2, while greatly reducing the charges collected on Columns 6 and 7, the former by a factor of nearly 3. The order of arrival has also changed, with Row 2 arriving before Column 7. The complex time structure of the traces can be understood by looking at the projection and noting that, due to the particular projection of the track onto the anode, parts of the Row 2 charge arrive both before and after the Column 7 charge. In noting changes in the traces with track translation, it is also worth noting that a translation of a full 10 mm, the pitch of the anode, will produce identical traces, but with the electrode numbers incremented appropriately by 1.

Figures 6A–6C document the trace changes that result from changing the angle θ by increments of 10° relative to a (7.13, 5.00, 32, 20) track. What is interesting here is that, while the ±10° motions produce fairly large changes in trace amplitudes compared with the central trace, they are not nearly so different from each other. Whether these cases could be distinguished by pulse amplitude alone will depend upon what signal-to-noise we can achieve in the detector. However, when we look at times of arrival, the two cases are clearly distinct, with the order of charge arrival being (2, 1, 7, 6) in the $\theta = 22°$ case and (7, 2, 1, 6) in the $\theta = 42°$ case. We also note the particular details of the trace shapes also vary considerably. However, until we know more about what signal-to-noise we can obtain, we do not wish to speculate about whether this information will also be usefully available to aid in our analysis.

Figures 7A–7C document the trace changes that result from changing the angle ϕ by increments of ±10° relative to a (7.13, 5.00, 32, 30) track. These variations produce even larger changes in the output traces than do the other two cases, primarily because changing ϕ effectively changes the projected track length, which changes the number of electrodes that collect induced charge. Thus, in addition to the observed changes in collected charge on Rows 1 and 2 and on Columns 6 and 7, between $\phi = 30°$ and $\phi = 20°$, we also see collected charge disappear from Column 8, whereas, between $\phi = 30°$ and $\phi = 40°$, we also see collected charge appear on Row 3. We further notice that the *range* of arrival times collapses as the angle ϕ increases and the range of distances between track segments and the anode similarly collapses.

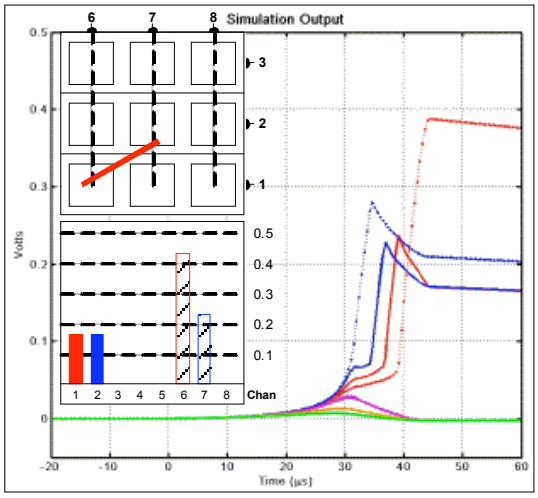

Figure 5A. Traces from a (2.87, 5.00, 32, 20) track.

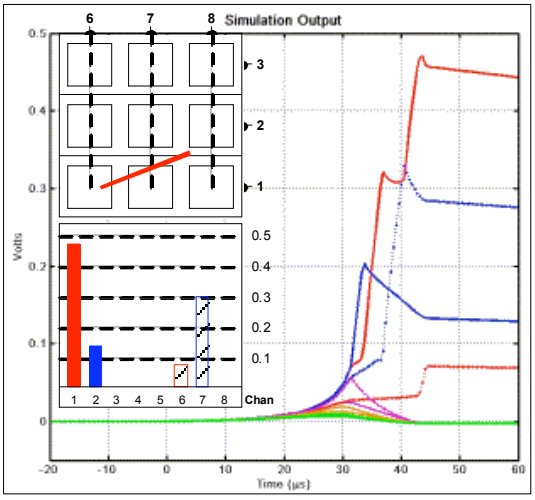

Figure 6A. Traces from a (7.13, 5.00, 22, 20) track.

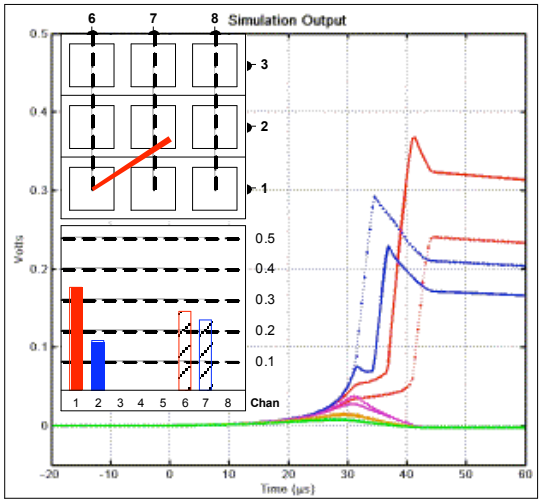

Figure 5B. Traces from a (5.00, 5.00, 32, 20) track.

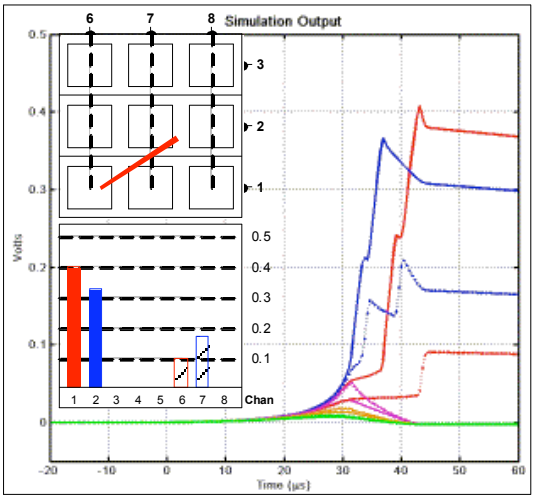

Figure 6B. Traces from a (7.13, 5.00, 32, 20) track.

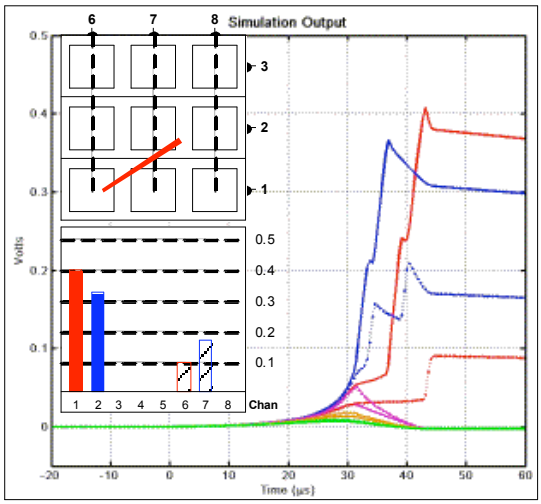

Figure 5C. Traces from a (5.00, 7.13, 32, 20) track.

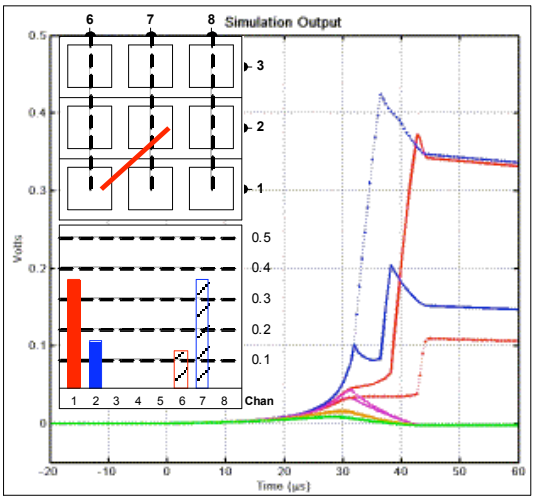

Figure 6C. Traces from a (7.13, 5.00, 42, 20) track.

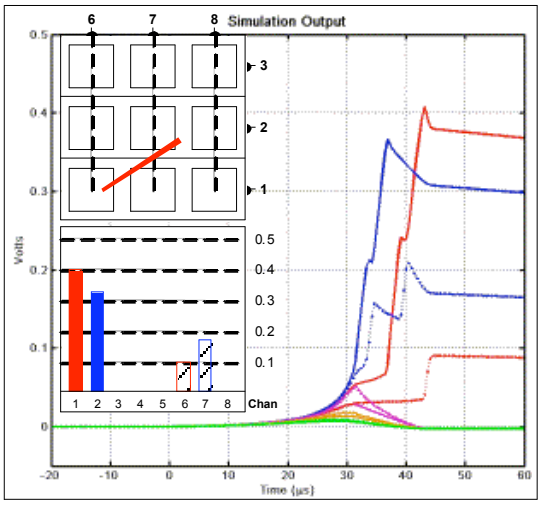

Figure 7A. Traces from a (7.13, 5.00, 32, 20) track.

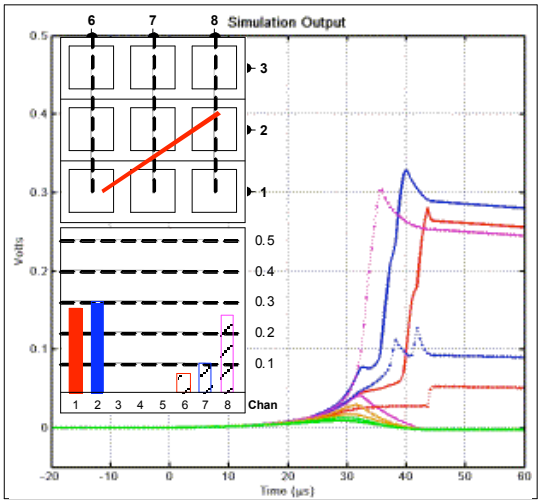

Figure 7B. Traces from a (7.13, 5.00, 32, 30) track.

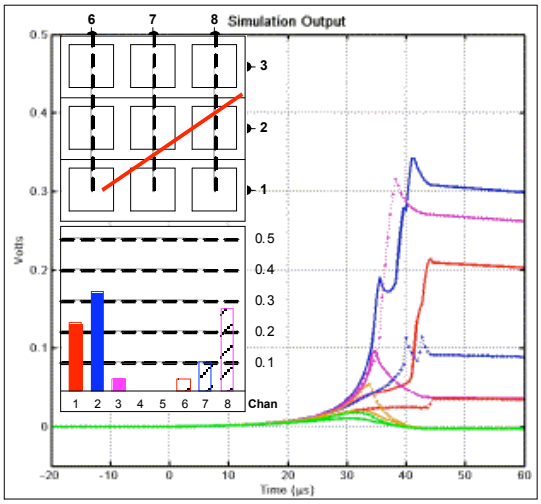

Figure 7C. Traces from a (7.13, 5.00, 32, 40) track.

Results—Analysis

The large trace changes observed from track translations of less than 1/4th of the anode pitch imply that the TPC method is sensitive enough to allow us to be able to easily detect and extract track locations with a precision that is significantly smaller than the strip pitch and may even approach 1 mm for 10 mm pitch strips. We further observe that, if in addition, we also use time of arrival information, we can significantly extend our capability to determine track locations. We therefore consider how captured traces might best be analyzed to extract track locations and orientations.

Since, in general, the further a charge drifts toward an electrode the more charge it induces, we might not expect there to be any simple relationship between the amount of projected charge under an electrode and the final charge induced on it. We have discovered, however, that due to the small pixel effect noted above, this generalization is not true in the present design. Thus, because a given electrode does not begin to effectively "see" a drifting charge segment until it is within about 5 cm, all charge segments have effectively identical drift lengths (i.e., 5 cm) and induce charges on the electrodes that are strictly proportional to their own charge. As a result, we find that the preamplifier signal amplitudes just after all charges have finished drifting (i.e., at 45 μs) are directly proportional to the charges in the track projected onto their respective electrodes. As an example, we look at Figure 4, where the ionization track has projected charge only on Rows 1 and 2 and Columns 6 and 7. Table 1 shows the measured voltages at 45 μs, their values normalized to unity, and the projected fractions of the tracks over the same electrodes. As may be seen, the agreement between the normalized and projected values is very good.

Table 1. Comparison of measured signal values to projected track lengths in Figure 4

Electrode	Measured Trace at 45 μs	Normalized Trace at 45 μs	Projected % Track on Electrode
#1	0.1118	0.118	0.12 ± 0.01
#2	0.1397	0.140	0.14 ± 0.01
#6	0.2973	0.314	0.32 ± 0.01
#7	0.4044	0.428	0.42 ± 0.01

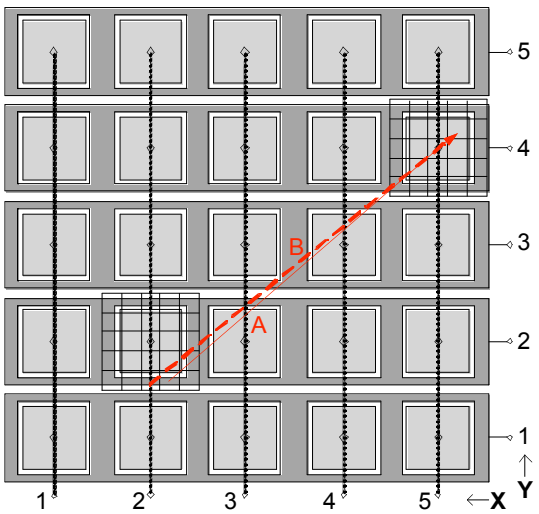

Figure 8. Method for generating tracks and projected charges for fitting to experimental data.

The result established in Table 1 is very important to our analysis because it means that we can use simple geometric analysis to extract track locations from signal traces. Figure 8 shows the proposed method. First we establish the Row-Column intersections where the track starts and stops. In Figure 4 this would be Row 1/Column 6 and Row

2/Column 7 and use times of arrival to establish which end was up (here Row 2/Column 7). We then compute the normalized trace fractions for each electrode as in Table 1. We then divide the starting and stopping intersections into a grid of squares of desired spatial resolution (here 2 mm). For each pair of starting and stopping squares we then geometrically compute the projected track on the electrode and make a weighted least squares comparison of these values to our measured values and select the globally best value as our best estimate of the track location. As may be seen by the comparison between tracks A and B in the figure, and their projections onto the electrodes, we expect the differences between the various tracks to be easily discernable.

CONCLUSIONS AND RECOMMENDATIONS

We have developed a computer model, based on the principles of electrostatics, that accurately produces expected output signals as the electrons in charge tracks generated in N_2 by alpha particles drift to our crossed strip anode. Our examination of these signals suggests that it will be possible to locate the origins of the trajectories of these tracks with an accuracy of better than 0.5 cm within a counter large enough to hold an entire RASA filter. Noting that Rn decay products will only emit one or two alpha particles, we can use the intersections of a larger number T of tracks (e.g., 3) to locate fission fragments or other radioactive particles trapped in the filters. Thus, by employing the number T as a "spatial coincidence" test, we can greatly reduce the counter's random background and enhance its sensitivity to even very tiny fission fragments.

At XIA we are continuing to develop this counter with the remainder of our Phase I SBIR funding and expect to have a small prototype working within the next 2–3 months, at which time we will be able to make first comparisons between the model traces presented here and actual traces captured from a counter with real electronics and their concomitant noise sources.

REFERENCES

Barrett, H. H., J. D. Eskin, and H. B. Barber (1995). Charge transport in arrays of semiconductor gamma-ray detectors, *Phys. Rev. Lett.* 75: 156–159.

Bowyer, S. M., H. S. Miley, R. C. Thompson, and C. W. Hubbard (1997). Automated particle sampler for Comprehensive Test Ban Treaty verification (The DOE Radionuclide Aerosol Sampler/Analyzer), *IEEE Trans. Nucl. Sci.* 44: 551–556.

Miley, H. S., S. M. Bowyer, C. W. Hubbard, A. D. Mckinnon, R. W. Perkins, R. C. Thompson, and R. A. Warner (1998). Automated aerosol sampling and analysis for the Comprehensive Test Ban Treaty, *IEEE Trans. Nucl. Sci.* 45: 1034–1039.

Warburton, W. K. (1998). An approach to sub-pixel spatial resolution in room temperature x-ray detector arrays with good energy resolution, in *Semiconductors for Room Temperature Radiation Detector Applications II*, R.B. James et al. (Eds.), *Mat. Res. Symp. Proc.* 487: 531–535.

Warburton, W. K., B. Dwyer-McNally, M. Momayezi, and J. E. Wahl (2004). Ultra-low background alpha particle counter using pulse shape analysis, in *Nuclear Science Symposium Conference Record, 2004 IEEE*, 1: 577–581. Digital Object Identifier 10.1109/NSSMIC.2004.1462261.

Warburton, W. K. and B. Dwyer-McNally (2006). Electronic background rejection in a new, ultra-low background alpha particle counter, *Nucl. Instrum. Methods Phys. Res. B* (accepted).